Carbohydrate Polymers 90 (2012) 23–33

Contents lists available at SciVerse ScienceDirect

Carbohydrate Polymers

journal homepage: www.elsevier.com/locate/carbpol

Molecular, mesoscopic and microscopic structure evolution during amylase digestion of maize starch granules

Ashok K. Shrestha[a,b,c], Jaroslav Blazek[c,d], Bernadine M. Flanagan[a], Sushil Dhital[a], Oscar Larroque[d,e], Matthew K. Morell[d,e], Elliot P. Gilbert[c], Michael J. Gidley[a,*]

[a] Centre for Nutrition and Food Sciences and ARC Centre of Excellence in Plant Cell Walls, The University of Queensland, Hartley Teakle Building, St. Lucia, Brisbane, Qld 4072, Australia
[b] School of Science and Health, University of Western Sydney, Hawkesbury Campus, Richmond, NSW, Australia
[c] Bragg Institute, Australian Nuclear Science and Technology Organisation, Locked Bag 2001, Kirrawee DSC, NSW 2232, Australia
[d] CSIRO, Food Futures National Research Flagship, Riverside Corporate Park, North Ryde, NSW, Australia
[e] CSIRO Division of Plant Industry, GPO Box 1600, Canberra, ACT 2601, Australia

ARTICLE INFO

Article history:
Received 9 January 2012
Received in revised form 10 April 2012
Accepted 12 April 2012
Available online 5 May 2012

Keywords:
Starch
Granule
Amylase
Amylose
Maize

ABSTRACT

Cereal starch granules with high (>50%) amylose content are a promising source of nutritionally desirable resistant starch, i.e. starch that escapes digestion in the small intestine, but the structural features responsible are not fully understood. We report the effects of partial enzyme digestion of maize starch granules on amylopectin branch length profiles, double and single helix contents, gelatinisation properties, crystallinity and lamellar periodicity. Comparing results for three maize starches (27, 57, and 84% amylose) that differ in both structural features and amylase-sensitivity allows conclusions to be drawn concerning the rate-determining features operating under the digestion conditions used. All starches are found to be digested by a side-by-side mechanism in which there is no major preference during enzyme attack for amylopectin branch lengths, helix form, crystallinity or lamellar organisation. We conclude that the major factor controlling enzyme susceptibility is granule architecture, with shorter length scales not playing a major role as inferred from the largely invariant nature of numerous structural measures during the digestion process (XRD, NMR, SAXS, DSC, FACE). Results are consistent with digestion rates being controlled by restricted diffusion of enzymes within densely packed granular structures, with an effective surface area for enzyme attack determined by external dimensions (57 or 84% amylose – relatively slow) or internal channels and pores (27% amylose – relatively fast). Although the process of granule digestion is to a first approximation non-discriminatory with respect to structure at molecular and mesoscopic length scales, secondary effects noted include (i) partial crystallisation of V-type helices during digestion of 27% amylose starch, (ii) preferential hydrolysis of long amylopectin branches during the early stage hydrolysis of 27% and 57% but not 84% amylose starches, linked with disruption of lamellar repeating structure and (iii) partial B-type recrystallisation after prolonged enzyme incubation for 57% and 84% amylose starches but not 27% amylose starch.

1. Introduction

Starch is the major source of dietary energy for humans, as well as being the main energy reserve for many plants. It is composed of two polymers of D-glucose, the largely linear amylose and extensively branched amylopectin, which are deposited as insoluble, semi-crystalline granules in plant storage tissues. Liberation of energy involves depolymerisation of starches with a suite of enzymes, the most prevalent being α-amylase which is usually responsible for the breakdown of macromolecules to oligosaccharide units that are then converted by other enzymes to glucose, the central fuel for many organisms. Starch granules display hierarchical structures spanning molecular (1–10 nm), mesoscopic (10–100 nm) and microscopic (100 nm–10 μm) length scales. Structural features at each of these length scales provide potential barriers to enzyme action and are therefore candidates for being the rate-determining factor that controls amylase digestion.

Within starch granules, amylose and amylopectin molecules are present in complex molecular arrangements that show structural periodicity of alternating crystalline and amorphous lamellae with a characteristic repeat distance of ca. 10 nm (Jenkins & Donald, 1996). Lamellar structures are hypothesised to form blocklets or

* Corresponding author. Tel.: +61 7 33652145; fax: +61 7 33651177.
E-mail addresses: m.gidley@uq.edu.au, mike.gidley@uq.edu.au (M.J. Gidley).

0144-8617/$ – see front matter © 2012 Elsevier Ltd. All rights reserved.
http://dx.doi.org/10.1016/j.carbpol.2012.04.041

super-helices that are arranged into longer range alternating amorphous and semi-crystalline radial growth rings of 120–400 nm thickness emanating from the hilum (Gallant, Bouchet, Buleon, & Perez, 1992; Oostergetel & van Bruggent, 1993). The structure of amylopectin involves clustering of branch points (Hizukuri, 1985) which predisposes branches to form double helices with each other that form the basis for semi-crystalline arrays. The amylose component, although more prone to form double helices from solution than amylopectin (Gidley & Bulpin, 1989), is not thought to be involved in extensive double helix formation within granules.

Native starch granules are considered to be protected from enzyme digestion by several factors such as dense packing and restricted mobility of polymer chains, together with double helical conformations of amylose molecules and long amylopectin branches as well as longer range structural features as reviewed previously (Bird, Lopez-Rubio, Shrestha, & Gidley, 2009; Zhang, Zihua, & Hamaker, 2008). Starch granules from the same species but differing in amylose/amylopectin ratio are known to differ in their enzyme resistance behaviour. For example, maize starch, which is available in a range of amylose contents from essentially zero to around 90%, has been reported to have enzyme-resistant starch contents from as low as 0.5% to almost 70% for granular forms (Morita, Ito, Brown, Ando, & Kiriyama, 2007; Shrestha et al., 2010). Depending on the amylose content, maize starches differ greatly in their morphological characteristics (Dhital, Shrestha, & Gidley, 2010; Jane, 2004; Planchot, Colonna, Gallant, & Bouchet, 1995), enzyme digestibility (Cairns, Sun, Morris, & Ring, 1995; Eerlingen, Deceuninck, & Delcour, 1993; Jiang, Campbell, Blanco, & Jane, 2010; Li, Jiang, Campbell, Blanco, & Jane, 2008; Morita et al., 2007; Sievert & Pomeranz, 1989; Themeier, Hollman, Neese, & Lindhauer, 2005), crystallinity and molecular order (Htoon et al., 2009; Lopez-Rubio, Flanagan, Shrestha, Gidley, & Gilbert, 2008), gelatinisation and pasting properties (Cooke & Gidley, 1992; Jane et al., 1999; Liu, Yu, Xie, & Chen, 2006; Russell, Berry, & Greenwell, 1989; Russell, 1987), chain length distribution (Srichuwong, Isono, Mishima, & Hisamatsu, 2005; Zhang, Ao, & Hamaker, 2006) and retrogradation behaviour (Eerlingen et al., 1993; Jiang & Liu, 2002; Miles, Morris, & Ring, 1985). Despite a wealth of information available on physicochemical and molecular structure of maize starch cultivars, only a few studies have linked the structure of these starches in the granular form at different length scales to their enzyme susceptibility (Evans & Thompson, 2004; Zhang et al., 2006).

The objectives of this study were to: (1) compare *in vitro* digestion behaviour of granular starches varying in amylose content at various time intervals, (2) monitor the progression of micro-structural changes, thermal behaviour and crystalline/lamellar/molecular order in granular starches during *in vitro* digestion and (3) establish the mechanistic basis for the effect of maize starch amylose content on enzyme resistance of granules based on structural changes at nm and μm scales during digestion. Zhang et al. (2006) provided evidence for the side-by-side digestion of amylose and amylopectin as well as crystalline and amorphous components in regular maize granules. Evans and Thompson (2004) characterised molecular and microscopic features after amylase digestion of high amylose maize starches and concluded that susceptible (regions within) granules were degraded whilst other granules appeared unaffected. We now extend these studies by reporting the effects of partial enzyme digestion of three types of maize starch granules on amylopectin branch length profiles, double and single helix contents (from NMR spectroscopy and related to differential scanning calorimetry data), crystallinity (wide angle X-ray scattering) and lamellar periodicity (small angle X-ray scattering). Comparing results for three maize starches that differ in both structural features and amylase-sensitivity allows conclusions to be drawn concerning the rate-determining features operating under these digestion conditions.

2. Experimental

2.1. Materials

Two high amylose maize starches (HAMS), Gelose 50 (G50) and Gelose 80 (G80), and a regular maize starch (RMS) were purchased from Penford Australia Ltd., Lane Cove, Sydney, Australia. The moisture content of RMS, Gelose 50 and Gelose 80, as measured by overnight vacuum drying at 70 °C, were 11.9, 12.3 and 13.2%, respectively. All samples were kept in a sealed container at room temperature. The apparent amylose contents of RMS, Gelose 50 and Gelose 80 were found to be 27.1, 57.5, and 83.6%, respectively, using an iodine colorimetric method as described previously (Htoon et al., 2009).

The following enzymes and chemicals were obtained from local distributors: α-amylase (Sigma A-3176 Type VI-B from porcine pancreas), pepsin (Sigma P-6887), pancreatin (Sigma P-1750 from porcine pancreas), α-amylase (3000 U/mL, Megazyme E-BLAAM from *Bacillus licheniformis*), amyloglucosidase (3200 U/mL, Megazyme E-AMGDF), enzyme glucose reagent (TR15104, Thermoelectron), isoamylase from *Pseudomonas* sp. (250 U/mL, Megazyme), APTS or 8-amino-1,3,6-pyrene trisulfonic acid (Sigma), Wizard mini column (Promega, Australia), Pullulan (P-82, Lot 80101, Shodex) and poly(ethylene oxide) standards (WAT 035711) (Polymer Standard Service, RI, USA). Freshly prepared distilled de-ionised water was used for reagent preparation as well as for sample analysis.

2.2. Enzyme digestion

The *in vitro* enzyme digestion of maize granules and enzyme-resistant starch determinations followed the method described previously (Htoon et al., 2009). In brief, the method involved initial treatment of starch with artificial saliva [α-amylase (Sigma A-3176) in carbonate buffer at pH 7.0] in carbonate buffer followed by acidification and digestion with pepsin. The neutralised starch mass was further incubated with pancreatin and amyloglucosidase at pH 6.0 for 0.0, 0.5, 1.5, 4.0, 8.0 or 24 h. The supernatant was removed at the end of the chosen incubation time by centrifugation and analysed for glucose content. The undigested residue left after centrifugation was freeze dried, weighed and divided by original weight to calculate % yield.

2.3. Differential scanning calorimetry (DSC)

DSC 1 (Mettler Toledo, Schwerzenbach, Switzerland) with internal coolant and nitrogen/air purge gas was used to determine gelatinisation/melting temperatures for raw starches as well as undigested residues from different incubation times. DSC was calibrated for the heat flow and melting temperature using indium and zinc as standards. An empty steel crucible was used as a reference. 30 μL capacity high pressure steel crucibles including a lid (part no. MT 51140403) and a gold plated copper sealer (part no. MT 51140403) were used to ensure hermetically sealed conditions for the hydrated starch. Starch (ca. 4 mg) and deionised water (ca. 12 mg) were accurately weighed directly into the crucible (starch to water ratio about 1:3), mixed to ensure good dispersion, and the crucible immediately covered with a gold coated seal followed by screwing the lid for final sealing. The crucible was left for about 30 min to ensure complete hydration of the sample before analysis. All analyses were carried out in duplicate. Thermal scanning was performed by heating the sample from 20 °C to 180 °C at 5 °C/min. The thermal transition temperatures and enthalpies of starches and digestion residues are reported as onset, peak, end and ΔH (J/g) as calculated by Star^e Software version 9.1 (Mettler Toledo).

2.4. X-ray diffraction (XRD)

XRD measurements of samples were made with a Panalytical X'Pert Pro diffractometer. The instrument was equipped with a copper X-ray generator ($\lambda = 1.54$ Å), programmable incident beam divergence slit and diffracted beam scatter slit, and an X'celerator high speed detector. X-ray diffraction patterns were acquired at room temperature over the 2θ range of 2° to 40° with a step size of 0.0330° 2θ and a count time of 400 s per step.

Assuming a constant divergent slit and a flat-surfaced sample of semi-infinite depth during XRD measurement, the experimentally obtained diffractograms were decomposed into a series of discrete diffraction peaks (corresponding to the crystalline phase) and two or three broad peaks (corresponding to the amorphous phase) using the modified curve-fitting procedure of Lopez-Rubio, Flanagan, Gilbert, & Gidley (2008). Crystallinity was calculated as the percentage proportion of the area under the crystalline peaks to the total area, which was calculated as the area between the experimental data and the baseline. The baseline was determined by collecting a diffractogram from an empty sample holder corresponding to the scattering from the instrument and air. The proportion of V-type crystallinity was determined as the area under the crystalline peaks at 7, 13 and 20° 2θ divided by the total minus the baseline area. Repeat analyses indicated an accuracy of ±1% for crystallinity values.

2.5. Small angle X-ray scattering (SAXS)

The application of this technique to starch systems has been reviewed previously (Blazek & Gilbert, 2011). Measurements were obtained on native and digested samples using a Bruker NanoStar SAXS instrument Cu K_α radiation of wavelength 1.5418 Å and point focus geometry. The optics and sample chamber were under vacuum to minimise air scattering. The sample to detector distance was 700 mm, which provided a q-range from 0.014 to 0.430 $Å^{-1}$. The q resolution of the instrument at the main lamellar peak at 0.065 $Å^{-1}$ was calculated to be 0.001 $Å^{-1}$. Samples were presented in 2 mm sealed quartz capillaries as suspensions containing excess water above the sedimented sample and scattering was measured for 60 min. Scattering data were background corrected and radially averaged as reported previously (Blazek & Gilbert, 2010). The fitting of the data was carried out using the iterative approach described in Section 3.

2.6. Solid state ^{13}C nuclear magnetic resonance (NMR) spectroscopy

Solid starch samples were analysed by ^{13}C NMR spectroscopy before and after enzyme digestion using the spectral acquisition and interpretation methodology described in Tan, Flanagan, Halley, Whittaker, & Gidley (2007). The solid-state ^{13}C CP/MAS NMR experiments were performed at a ^{13}C frequency of 75.46 MHz on a Bruker MSL-300 spectrometer. Double and single helix contents are considered to be accurate to ±1% based on repeat analyses.

2.7. Scanning electron microscopy (SEM)

For SEM, the dried starch powder was thinly spread onto circular metal stubs coated with double-sided adhesive carbon tape. The stubs were transferred to a desiccator containing P_2O_5, placed under vacuum and left overnight at room temperature. The powder on the stubs was platinum coated in an Eiko IB-5 Sputter Coater (at 6 mA, 5 min for medium coating) in an argon gas environment, yielding approximately 15 nm coating thickness. The coated samples were imaged in a JEOL 6400 JSM Scanning electron microscope (JEOL Ltd., Tokyo, Japan). The accelerating voltage used was 10 kV and the working distance was set at 15 mm. Representative micrographs were taken at low magnification followed by higher magnification up to 20,000 times.

2.8. Fluorophore assisted carbohydrate electrophoresis (FACE)

Raw starches and their enzyme-digested residues were gelatinised and debranched by isoamylase according to Castro, Ward, Gilbert, & Fitzgerald (2005). The isoamylase digestion of starches produces a population of linear oligosaccharides with a degree of polymerisation between 3 and 85 which can be resolved by capillary electrophoresis (Morell, Samuel, & O'Shea, 1998; O'Shea, Samuel, Konik, & Morell, 1998). These debranched starches were labelled with APTS (8-amino-1,3,6-pyrenetrisulfonic acid) solution following previously published literature (Castro et al., 2005; Morell et al., 1998; O'Shea et al., 1998).

Capillary electrophoresis of APTS labelled oligosaccharides to determine the branch length profile (O'Shea et al., 1998) was performed on a P/ACE 5010 capillary electrophoresis system (Beckman Coulter, Gladesville, NSW, Australia) with argon-LIF detection. The longer chain lengths in the samples (>DP 80), e.g., amylose chains, cannot be detected by this system, thus this analysis of the debranched starch is principally an analysis of debranched amylopectin (Morell et al., 1998).

3. Results and discussion

3.1. Enzyme digestibility of maize starch granules

The recovered yields of insoluble partially digested starches after incubation of granules with amylase for 0.5, 1.5, 4.0, 8.0 and 24.0 h are shown in Table 1. There is a clear difference in behaviour between maize starch of 27% amylose (RMS) which is digested relatively rapidly, and those with 57% (G50) or 84% (G80) amylose which are digested at similar rates but much slower than RMS. Likewise, the enzyme-resistant starch contents determined *in vitro* were 0.5, 47.8 and 52.1% (dry basis) for RMS, G50 and G80, respectively. The similarity in enzyme resistance for maize starches of greater than 50% amylose has been shown previously (Morita et al., 2007) as has the faster digestion of regular maize starch (Jiang & Liu, 2002; Zhang et al., 2006). The commonly stated association that resistance to enzyme digestion increases markedly with amylose content does not hold for granular forms of maize starch. For example Evans and Thompson (2004) reported similar *in vitro* resistant starch contents (essentially a single point measurement of the digestion profile) for amylose extender V and VII maize starch granules of 66.0 and 69.5%, respectively. In a more extensive study, Morita et al. (2007) showed that both *in vitro* and *in vivo* RS contents for maize granules were higher for maize granules of 54% amylose than 90% amylose. In terms of digestibility *in vivo*, regular maize starch granules are considered to undergo slow but essentially complete digestion in the small intestine whereas granular high amylose maize starches are incompletely digested in the small intestine and so contribute to the nutritionally beneficial resistant starch that is fermented in the colon (Bird et al., 2009). The quantitative comparison of digestibility values for uncooked granules between studies, even for the same starch, however, is difficult as methodology, number, type and dosage of enzymes employed markedly affect the digestion rate (Goni, Garcia-Diz, Manas, & Saura-Calixto, 1996; Planchot et al., 1995).

3.2. Crystallinity by X-ray diffraction

As expected, RMS (27% amylose) displayed an A-type crystalline diffraction pattern with the main diffraction doublet at 17 and 18° 2θ and peaks at 15, 20 and 23° 2θ. High-amylose starches, on the

Table 1
Percentage yield of undigested residues from granular starches after various enzyme incubation times.[a,b]

Samples	Incubation times, h				
	0.5	1.5	4	8	24
Regular maize starch	75.1 ± 0.6	45.3 ± 0.1	12.6 ± 1.6	5.9 ± 0.4	3.1 ± 1.0
Gelose 50	91.7 ± 0.0	86.5 ± 0.1	80.7 ± 0.0	74.9 ± 0.3	67.5 ± 1.0
Gelose 80	83.3 ± 1.0	80.1 ± 5.9	74.4 ± 5.9	70.8 ± 0.5	63.2 ± 5.9

[a] All data are expressed as moisture free basis.
[b] Mean ± standard deviation (of duplicates).

other hand, showed B-type crystallinity, characterised by a strong diffraction peak at 17° 2θ and weaker reflections at 15, 19.5, 22 and 24° 2θ (Fig. 1). The B-type crystalline pattern of high-amylose maize starches is thought to originate from longer amylopectin branches compared to regular maize. These longer amylopectin branches may also contribute to other properties inherent to high-amylose cultivars such as iodine binding used to measure amylose contents; hence, apparent amylose contents are typically reported.

Starch molecules in a crystalline alignment give rise to the peaks in X-ray diffractograms, whereas starch molecules in amorphous regions contribute to the diffuse regions of the XRD patterns. Powder X-ray diffraction or wide-angle X-ray scattering is widely used to quantify starch crystallinity by comparing the integrated intensity of the amorphous pattern to that of the crystalline peaks. The critical step in determining the crystallinity of starch is the separation of the crystalline peaks from the amorphous region. Traditional background estimation based on drawing a smooth curve from tail to tail following the general scope of the continuous background has recently been improved by introducing a peak-fitting procedure as used in the present study (Lopez-Rubio, Flanagan, Gilbert, et al., 2008) or an iterative smoothing algorithm (Frost, Kaminski, Kirwan, Lascaris, & Shanks, 2009). Comparison of X-ray diffraction patterns of native and partly digested starches of the three maize varieties used in this study showed differences in the effect of α-amylolysis on the crystalline architecture of starch granules. Based on the available time points of α-amylolysis, RMS digestion caused the amorphous portion of the diffractogram to decrease slightly compared with crystalline peaks resulting in a small increase of crystallinity from 30.0 to 34.5%. This was due primarily to an increase in V-type crystallinity (diffraction peaks at 7, 13 and 20° 2θ) from 1.9 to 5.4% (Table 2), suggesting that, for the relatively rapid digestion of RMS, crystalline V-type structures are more resistant than either crystalline double helical or amorphous segments to enzyme digestion.

As apparent from Fig. 1, there was a significant effect of the first 30 min of digestion on the crystalline structure of HAMS. The most noticeable change was the lower intensity of the peak at 5.5° 2θ in both Gelose 50 and Gelose 80 in 0.5 h digested samples compared to native starches. However, this is not an effect of enzyme digestion as the same change was found for starches treated under identical conditions without addition of enzyme (data not shown). It is likely that hydration and subsequent drying processes have resulted in

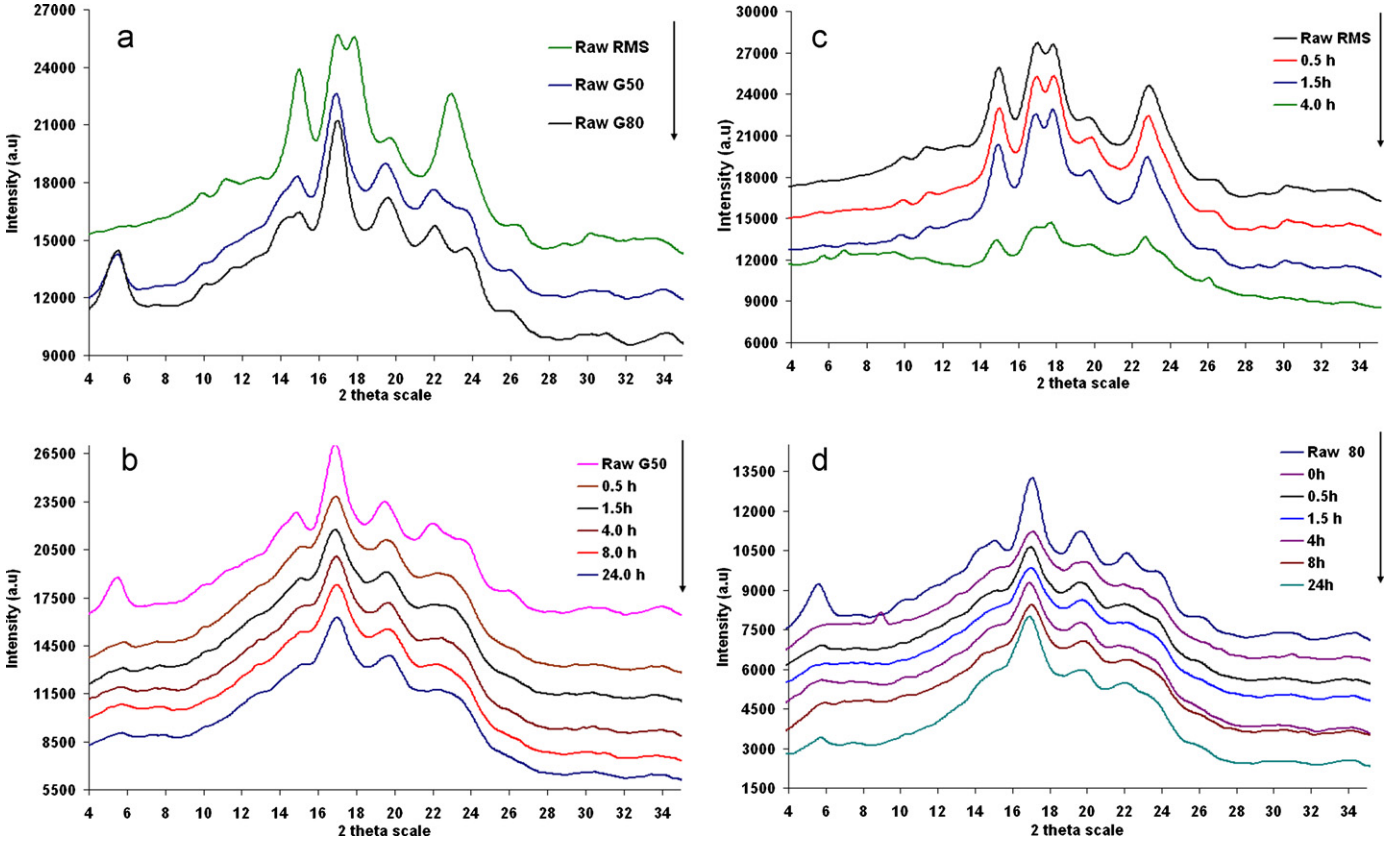

Fig. 1. XRD patterns of uncooked starches used in this study (a), enzyme digested residues of regular maize starch (RMS) (b), Gelose 50 (G50) (c) and Gelose 80 (G80) (d) after various enzyme incubation times. Curves are offset for clarity.

Table 2
Percentage of XRD crystallinity and SAXS fitting parameters of raw and enzyme digested residues from RMS and HAMS as a function of enzyme incubation time.

			Native	0.5 h	1.5 h	4 h	8 h	24 h
Regular maize starch	XRD	Crystallinity type	A	A	A	–	–	–
		% Total crystallinity	30.0	33.3	34.5	–	–	–
		% V-type crystallinity	1.9	5.1	5.4	–	–	–
	SAXS	Exponent of powerlaw	2.6	2.8	3.1	2.41	–	–
		Prefactor of the powerlaw	16.3	13.7	2.2	117	–	–
		Lamellar peak intensity/1000	333.0	202.0	93.0	133	–	–
		Lamellar peak position	10.1	10.1	10.1	10.1	–	–
		Width of the lamellar peak	0.0	0.0	0.0	0.027	–	–
Gelose 50	XRD	Crystallinity type	B	B	B	B	B	B
		% Total crystallinity	27.4	25.2	27.1	26.5	30.2	30.5
		% V-type crystallinity	2.1	2.7	2.7	2.7	2.8	2.7
	SAXS	Exponent of powerlaw	2.23	2.21	2.24	2.28	2.41	2.64
		Prefactor of the powerlaw	79.7	196.9	187.2	169.8	87.2	30.2
		Lamellar peak intensity/1000	147	110	107	118	117	123
		Lamellar peak position	10.0	10.0	10.0	10.0	10.0	10.0
		Width of the lamellar peak	0.036	0.03	0.03	0.033	0.038	0.042
Gelose 80	XRD	Crystallinity type	B	B	B	B	B	B
		% Total crystallinity	23.2	22.5	21.7	21.0	25.1	24.1
		% V-type crystallinity	2.1	2.2	1.9	2.0	2.1	2.1
	SAXS	Exponent of powerlaw	1.95	1.94	2.12	2.14	2.17	2.19
		Prefactor of the powerlaw	349.5	270.6	334.9	341.6	348.9	221.7
		Lamellar peak intensity/1000	117	120	77	80	86	57
		Lamellar peak position	10.0	10.0	10.0	10.0	10.0	10.0
		Width of the lamellar peak	0.032	0.042	0.023	0.023	0.023	0.023

disruption of the crystalline register of helices as suggested by the side chain liquid crystalline model for starch (Waigh, Perry, Riekel, Gidley, & Donald, 1998). In line with a previous report (Lopez-Rubio, Flanagan, Shrestha, et al., 2008), the crystallinity of native Gelose 50 and Gelose 80 was determined to be 27.4 and 23.2%, respectively, of which approx. 2% was V-type crystallinity (Table 2). Enzymatic digestion caused little change in the crystallinity of Gelose 50 up to 4 h digestion (25–27%), after which the crystallinity increased slightly up to 30% following 24 h of digestion (Table 2). For Gelose 80, there was little difference in either B-type (21–25%) or V-type (2%) crystallinity throughout digestion.

For all three starches, the fact that crystallinity neither increased nor decreased significantly during digestion is consistent with the concept of side-by-side digestion of crystalline and amorphous regions for both the relatively rapidly digested RMS (Zhang et al., 2006) and the much slower digested Gelose 50 and Gelose 80. This could be caused by the rapid digestion of only selected (regions of) granules leaving undigested regions in the native form. For digestion of Gelose 50 and 80 at early stages there is evidence from microscopy for granule to granule variation in digestion (see Section 3.6), although more extensive digestion involves most if not all granules after 24 h digestion. However, even if there is granular selectivity, digestion of crystalline and non-crystalline regions within these enzyme-susceptible regions is sufficiently simultaneous that there are no overall changes in crystallinity. Two secondary effects were noted. For RMS, there was an increase in V-type crystallinity after 0.5 h digestion (recovered yield 75% – Table 1) that was not seen for Gelose 50 and Gelose 80 after a similar extent of digestion (8 h and 4 h, respectively – Table 1). For Gelose 50, there was evidence for a small increase in B-type crystallinity after 8 or 24 h, suggesting that some recrystallisation occurs, as has previously been demonstrated for extruded high amylose maize (Lopez-Rubio, Flanagan, Shrestha, et al., 2008).

3.3. Small angle X-ray scattering

SAXS curves from native and partly digested starches were characterised by intense scattering at low scattering vector (q), which rapidly decreased at larger angles and featured three scattering peaks: a lamellar peak around q of 0.06 Å^{-1}, a broad second order reflection peak around 0.12–0.13 Å^{-1} and the 100 interhelix peak around 0.4 Å^{-1} corresponding to the distance between the 100 crystallographic planes in the hexagonal unit cell of B-crystalline starch (Fig. 2). As the thickness of the capillaries varied slightly and the packing density and water content of the sample in the capillary were unknown, the scattering curves were not on an absolute scale. In order to enable better comparison between the samples, the SAXS curves were normalised based on matching the intensity of the XRD curve for each given sample as indicated in Fig. 2.

Scattering data were fitted to a function as described previously representing a combination of a power-law term and multiple peaks (Blazek & Gilbert, 2010). The power-law function accounts for the scattering arising from structures of larger length-scale than lamellae including interfaces. The lamellar peak around 0.06 Å^{-1} was fitted to the function comprising the sum of a Lorentzian peak and a Gaussian peak with identical peak centre, intensity and width. A second reflection peak around 0.12 Å^{-1}, where applicable, was fitted to a single Gaussian peak. The overall equation is as follows:

$$I(q) = k \cdot \frac{I_{01}}{1 + (2(q - q_{01})/B_1)^2} + (1 - k) \cdot I_{01} \exp\left[-\frac{(q - q_{01})^2}{2B_1^2}\right] + I_{02} \exp\left[-\frac{(q - q_{02})^2}{2B_2^2}\right] + Aq^{-\delta} + Bkgd$$

where the first term is a Gaussian function and the second is a Lorentzian in which I_0 is the peak height, q_0 is the position of centre of the peak, and the B term is related to the full width at half maximum of the peak. The third term is the Gaussian peak, which fits the second order reflection. The fourth term represents a power-law where A is the prefactor and δ is the exponent of the power-law function. The Bragg spacing d was calculated from the position of the peak according to $d = 2\pi/q_0$.

Fitting parameters are shown in Table 2. In line with results of Blazek and Gilbert (2010) RMS displayed a significantly more defined lamellar peak in comparison to the high-amylose varieties (333 arbitrary units (a.u.) for RMS compared to 147 and 117 a.u. for Gelose 50 and Gelose 80, respectively), and was also better fitted with the function used than the high-amylose varieties. Scattering data from RMS showed decreasing lamellar peak intensity within the first 1.5 h of digestion followed by a small intensity increase at

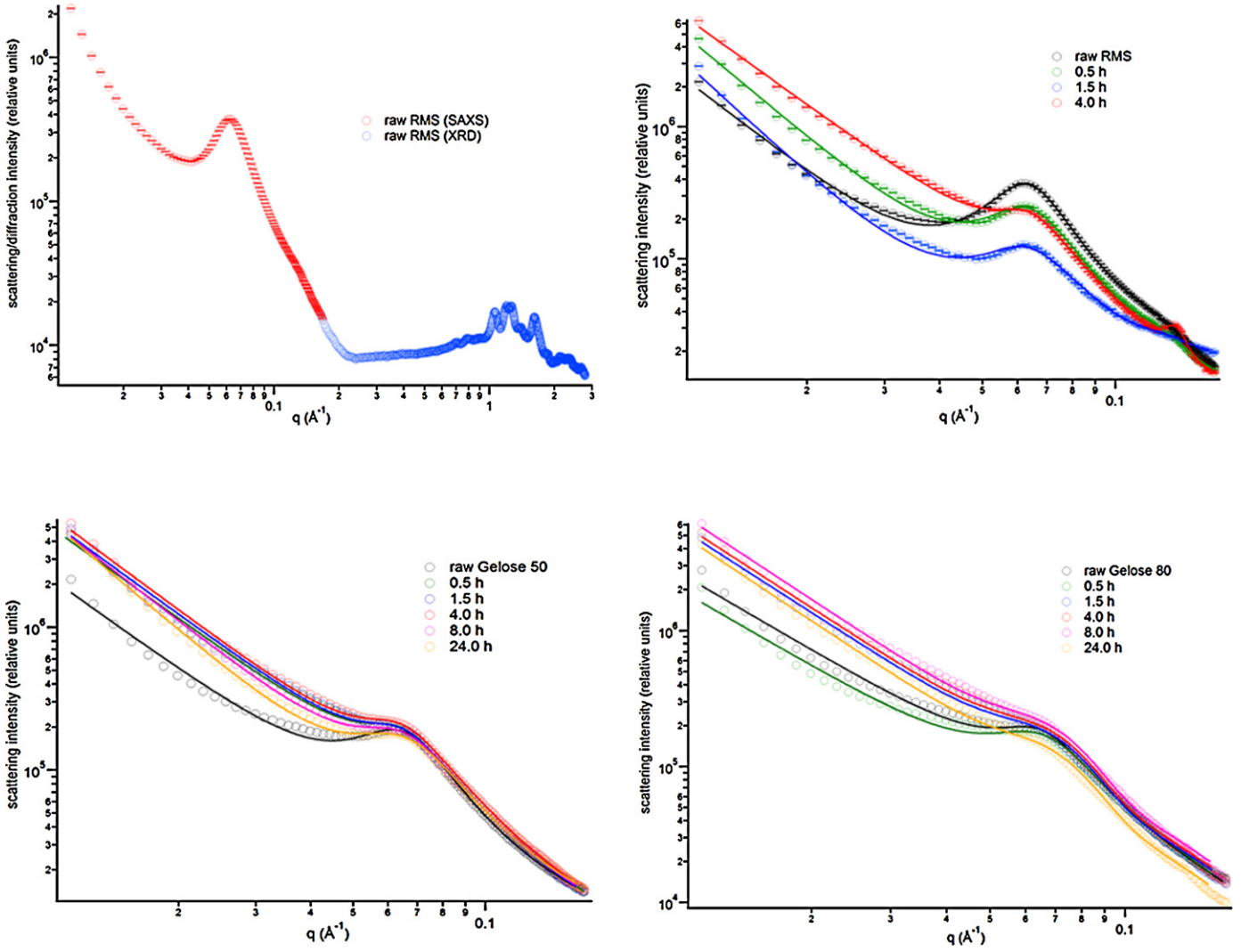

Fig. 2. SAXS curves of starches used in this study: combined XRD and SAXS data for regular maize starch (RMS) (a), SAXS curves of native and partly digested RMS (b), SAXS curves of native and partly digested Gelose 50 (c), SAXS curves of native and partly digested Gelose 80 (d). Fits are represented by solid lines.

the 4 h time point (Table 2, Fig. 2); the peak position did not change significantly. As apparent from Fig. 2, the peak around 0.12 $Å^{-1}$ remained essentially unchanged during the first 1.5 h of digestion but became significantly more defined in the sample after 4 h of digestion; this feature can be fitted by a Gaussian peak with peak centre at 0.135 $Å^{-1}$, which corresponds to a *d*-spacing of 4.6 nm.

Gelose 50 and Gelose 80, the two B-type starches used in this study, produced more complex scattering than A-type RMS, and could not be well described with a simple power law and single peak algorithm. This difficulty seems to be caused by increased scattering at *q* values below the lamellar peak (between 0.03 and 0.05 $Å^{-1}$) and was observed previously (Blazek & Gilbert, 2010) for Hylon VII starch. Both high-amylose starches displayed broader and less defined lamellar peaks than RMS and lacked the second-order reflection peak around 0.12 $Å^{-1}$. To enable better comparison among samples during the course of digestion, the position of the lamellar peak was fixed during fitting at a position of 0.063 $Å^{-1}$. The intensity of the lamellar peak in Gelose 50 decreased from 147 a.u. to 110 a.u. in the first 0.5 h of digestion. From 1.5 h of digestion onwards, the peak intensity remained relatively constant (Table 2). For Gelose 80, the peak intensity remained essentially unchanged during the first 0.5 h of digestion followed by decrease at 1.5 h, after which it remained without significant changes up to 24 h, where it further decreased. Whilst a peak around 0.12 $Å^{-1}$ was not observed for Gelose 50 at any point during digestion, this peak became apparent in samples of Gelose 80 after 8 and 24 h of digestion (peak position of 0.135 $Å^{-1}$). This is consistent with structural reorganisation occurring after long digestion times. For Gelose 50, this seems to involve an increase in B-type crystallinity, whereas for Gelose 80 a feature on the length scale of 4–5 nm is formed as observed previously for the same starch after extrusion and extensive digestion (Lopez-Rubio, Flanagan, Gilbert, et al., 2008). Both Gelose 50 and Gelose 80 exhibit an inverse correlation between the intensity of the lamellar peak and intensity in the limit of low *q*. For Gelose 50, the intensity at low *q* increases in the first 0.5 h and then remains relatively constant throughout the remaining hydrolysis time; similarly the lamellar peak intensity decreases in the first 0.5 h and then remains relatively constant. The same behaviour is evident in Gelose 80 only here the increase/decrease occurs somewhat later at 1.5 h. The observed simultaneous decrease in the intensity of the lamellar peak and increase in the low-*q* scattering is consistent with a model in which preferential hydrolysis of the bulk amorphous starch occurs within the amorphous growth rings (Blazek & Gilbert, 2010). Although the exact location or nature of these growth rings is not defined discretely, they have a low polymer concentration and hence would be more likely to be accessible to enzyme attack. A relatively small number of enzyme actions may be sufficient to cause the observed change in lamellar peak intensity, particularly

as the X-ray diffraction data (Fig. 2, Table 2) provide no evidence for preferential digestion of amorphous over crystalline material as any increase in crystallinity with hydrolysis time is minor (Table 2). Analyses of residual amylopectin branch length profiles provide a potential molecular explanation for the initial changes in lamellar peak intensity (discussed below).

3.4. ^{13}C solid state NMR

^{13}C NMR spectra of solid starches can be deconvoluted to give quantitative estimates of the relative proportion of double (A, B-type) and single (V-type) helices. Results are shown in Table 3 as a function of enzyme digestion time. In all cases, values for total double helix content are similar or slightly (1–5%) higher than values of crystallinity from X-ray diffraction obtained using the imperfect crystallite model of Lopez-Rubio, Flanagan, Shrestha, et al. (2008) (Table 2). This shows that almost all double helices are present within (imperfect) crystallites for all samples. For single helices, values from ^{13}C NMR are all higher (2–5 times) than V-type crystallinity values from X-ray diffraction, showing that most single helices are not present in crystalline arrays and consistent with the dispersed and poorly organised nature of the amylose molecules that are the most likely origin of V-type helices within granules.

During digestion, there were only minor changes in helix contents for each of the three starches, which is consistent with the limited changes observed by X-ray diffraction. This shows that to a first approximation, enzyme digestion of not only crystalline and amorphous regions but also helical and non-helical regions occurs side-by-side. The minor changes occurring during digestion include an increase in double helix (B-type) content after 4 h and longer for Gelose 50 and Gelose 80 (Table 3a), consistent with the observation of greater crystallinity after 8 h for Gelose 50 (XRD; Table 2) and the formation of a structure on the 4–5 nm length scale in Gelose 80 (SAXS; Table 2). This suggests that there is either a recrystallisation process or (less likely) a preferential digestion of amorphous zones after long digestion times. There were no systematic changes in V-type single helix content during enzyme digestion (Table 3). This suggests that the increase in V-type crystallinity seen after 0.5 and 4 h for RMS (Table 2) was due to rearrangement of some pre-existing single helices into crystalline arrays during the digestion process.

3.5. Gelatinisation and melting of starch granules and enzyme digestion residues

Thermal characteristics of the gelatinisation of granular starches and their enzyme-digested residues are summarised in Table 4. As expected, the gelatinisation endotherms of RMS and HAMS are different, with a relatively narrow endotherm for RMS and broader endotherms for Gelose 50 and Gelose 80 with consequent uncertainties in defining onset and end temperatures, and therefore gelatinisation enthalpies. The gelatinisation peak temperature (GT) and enthalpy (ΔH) of raw RMS were 68 °C and 6.5 J/g, respectively, with additional endotherms at about 100 °C and occasionally above 140 °C. Similar gelatinisation characteristics for RMS have been reported by several investigators (Liu et al., 2006; Russell et al., 1989; Sievert & Pomeranz, 1990). The secondary endotherms at ≥90 °C have been attributed to the phase transition of amylose–lipid complexes (Biliaderis, Page, Slade, & Sirett, 1985; Jovanovich & Anon, 1999), whereas peaks ≥145 °C have been assigned to melting of amylose crystallites (Gidley et al., 1995; Russell, 1987). The endotherms of the enzyme digested residues from RMS showed that GT slightly increased and ΔH decreased with increasing incubation time (Table 3b). These results are in agreement with previous findings for potato starch and RMS (Blazek & Gilbert, 2010; Jiang & Liu, 2002). Sievert and Pomeranz (1990) also reported lower values for enzyme digested RS residues (52.8 °C GT and 0.96 J/g ΔH after 30 min incubation) for heat treated maize starch. However, Zhang et al. (2008) reported GT of 67 °C (peak) and ΔH of 10 J/g for normal maize starch and few changes in the endotherms after enzyme treatment from 20 to 120 min.

DSC thermograms of raw HAMS also showed a gelatinisation endotherm starting at about 70 °C which extended to higher temperatures than for RMS; onset and end temperature and ΔH values for Gelose 50 and Gelose 80 are similar to the values reported by Liu et al. (2006). The broad peak in HAMS is probably a consequence of the structural heterogeneity present, particularly at the granule level. Hot stage microscopy of HAMS shows a wide range of temperatures over which individual granules and regions within granules lose their birefringence (data not shown). HAMS also showed small endotherms (typically $\Delta H < 1$ J/g) at temperatures >140 °C indicative of amylose double helix melting. It is, however, not possible to determine whether amylose double helices were present within the original granule or whether they were formed in the DSC pan at temperatures above that required for granule gelatinisation.

DSC thermograms of enzyme digested residues from both HAMS showed similar broad transitions as their undigested counterparts (Table 3b). During the enzyme digestion process, there was a small increase in peak temperature for both HAMS, but no systematic trend in ΔH values. In a similar study, Jiang and Liu (2002) reported peak temperatures and enthalpies of 96.6, 95.0 and 99.2 °C and 16.7, 16.7 and 18.6 J/g for 0, 2 and 48 h digested residues from Hylon VII, respectively. Higher temperature endotherms (130–170 °C) were observed inconsistently for enzyme digestion residues from both starches, typically with a ΔH of less than 1 J/g, but rising to 1.5 J/g for 8 and 24 h residues from both Gelose 50 and Gelose 80. This suggests the possibility of limited amylose re-crystallisation during digestion, but again it is possible that re-crystallisation occurred during heating in the DSC pan.

Overall the DSC results showed a slight increase in gelatinisation temperature with enzyme treatment as reported by Blazek and Gilbert (2010), limited change in gelatinisation enthalpies with extent of digestion for HAMS as previously reported for both high amylose (Jiang & Liu, 2002) and regular maize starch (Zhang et al., 2006). The inconsistent observation of low enthalpy endotherms above 140 °C suggests that full length amylose double helices do not play a major role in causing the slow enzyme digestion of high amylose maize starch granules.

3.6. Microscopy

SEM images showed that starch granules from the three varieties vary in size with most below 20 μm in size, in agreement with published results (Jane, Kasemsuwan, Leas, Zobel, & Robyt, 1994). The SEM image of raw regular starch granules showed an irregular shape with sharp edges and a wrinkled surface with small pores (Fig. 3a). Amylase digestion for 1.5 h (48% starch digested) enlarged the existing surface pores due to internal corrosion by the enzyme (Fig. 3b). On subsequent digestion, the surface pores merged together forming larger channels/grooves resulting in hollow interiors ('inside out' digestion) (e.g. 4 h, about 80% digested). During the later stages of digestion, some intact granule fragments were observed alongside hollowed granules, probably arising from a minority of granules that have lower levels of pores as previously described (Zhang et al., 2006).

Both HAMS showed similar sizes with a range of irregular shapes (Fig. 3a) as reported previously by others (Jane et al., 1994; Planchot et al., 1995). The surface of Gelose 80 appeared smoother than that of Gelose 50. Gelose 50 and Gelose 80 were similarly susceptible to enzymatic digestion over 0.5–24 h of digestion (Table 1). SEM images of enzyme digested residues for the two starches were also similar. The early stages of HAMS digestion (0.5 h) were

Table 3a
Helical order (%) of starches before and after amylase digestion calculated from NMR.

Starch types	Type of helix/order (%)	Incubation times					
		0.0 h	0.5 h	1.5 h	4 h	8 h	24 h
Regular maize starch	Double helix (%)	33	33	34	30	NA	NA
	Single helix, V-type (%)	12	7	8	11	NA	NA
	Non-ordered (%)	55	60	58	59	NA	NA
Gelose 50	Double helix (%)	23	22	22	32	24	35
	Single helix, V-type (%)	12	8	9	8	11	9
	Non-ordered (%)	65	70	69	60	65	56
Gelose 80	Double helix (%)	21	20	22	23	26	28
	Single helix, V-type (%)	6	6	3	7	4	6
	Non-ordered (%)	73	74	75	70	70	66

NA, Not analysed due to insufficient sample.

Table 3b
Gelatinisation temperatures and enthalpies before and after amylase digestion from DSC.[a]

Starch types	DSC parameter	Incubation times					
		0.0 h	0.5 h	1.5 h	4 h	8 h	24 h
Regular maize starch	Onset, °C	68.3 ± 2.1	69.8 ± 2.3	70.6 ± 3.0	74.5 ± 1.5	NA[b]	NA
	Peak, °C	73.1 ± 1.9	75.0 ± 2.9	75.8 ± 2.7	79.5 ± 2.1	NA	NA
	End, °C	79.9 ± 2.9	81.6 ± 3.1	82.1 ± 3.1	86.0 ± 0.9	NA	NA
	Enthalpy, J/g	6.5 ± 0.7	5.3 ± 0.5	4.9 ± 0.6	4.0 ± 0.2	NA	NA
Gelose 50	Onset, °C	69.8 ± 1.9	68.0 ± 1.9	67.9 ± 1.5	68.1 ± 1.8	77.2 ± 2.1	70.7 ± 1.0
	Peak, °C	89.5 ± 2.8	79.7 ± 2.6	79.7 ± 3.0	79.6 ± 2.0	81.1 ± 2.1	81.5 ± 2.1
	End, °C	109.5 ± 3.2	106.1 ± 3.4	97.5 ± 3.5	105.2 ± 4.0	106.3 ± 3.1	105.4 ± 2.5
	Enthalpy, J/g	8.2 ± 0.9	13.1 ± 2.1	11.3 ± 1.5	11.3 ± 0.9	10 ± 0.9	9.5 ± 0.9
Gelose 80	Onset, °C	72.0 ± 2.4	70.4 ± 13	73.2 ± 1.9	72.2 ± 1.8	69.7 ± 1.3	89.1 ± 2.1
	Peak, °C	88.9 ± 3.0	90.5 ± 3.0	92.0 ± 2.8	84.2 ± 2.5	92.1 ± 3.2	95.0 ± 2.8
	End, °C	107.8 ± 3.5	106.6 ± 3.5	96.7 ± 2.9	91.6 ± 3.4	114.9 ± 4.6	108.9 ± 2.9
	Enthalpy, J/g	10.6 ± 1.1	5.0 ± 0.6	8.5 ± 0.9	4.1 ± 0.2	6.8 ± 1.9	5.1 ± 0.9

[a] Mean ± standard deviation (of duplicates).
[b] NA, Not analysed due to insufficient sample.

characterised by 'surface pitting' or 'exo corrosion', and 'surface scratching' (Fig. 3b). Further incubation (1.5 h) showed the channels and pores becoming larger in both types of granules. After 4 h incubation, it was obvious that unlike RMS, the digestion pattern in HAMS is markedly heterogeneous, i.e. some granules were apparently unaffected by amylases whereas others were significantly digested as previously described (Evans & Thompson, 2004). More heterogeneity was observed after 8 h of digestion with some Gelose 50 granules being almost completely hydrolysed along the channels, forming large holes deeper into the granules through 'endo corrosion', whereas other granules were only affected on the surface. Similarly, 8 h digestion of Gelose 80 (~30% digested overall) showed digestion along the furrows exposing the interior with several compartments. After 24 h incubation (~35% starch digestion) multiple patterns of attack resulted in numerous holes on the granule surface and some granules almost collapsed due to hydrolysis from the inside towards the periphery.

Table 4
The relative proportion (%) of debranched amylopectin chain lengths of regular maize starch and high amylose maize starches before and after amylase digestion for various times.

Digestion times	% Amylopectin chain lengths, degree of polymerisation			
	6–12	13–24	25–36	>36
Regular maize starch				
Raw	32.7	52.2	9.1	6
Digested 0.5 h	34.2	53.7	8.9	2.8
Digested 1.5 h	34.2	52.6	9.5	2.6
Digested 4.0 h	33.7	54.2	8.7	2.5
Digested 8.0 h	36.1	53.7	7.3	1.8
Digested 24.0 h	34.3	52.8	8.8	3.1
Gelose 50				
Raw	21.5	51.4	14	12.8
Digested 0.5 h	30.3	54.4	11.0	3.5
Digested 1.5 h	28.5	54.5	12.1	4.6
Digested 4.0 h	25.0	57.3	13.4	4.2
Digested 8.0 h	24.3	57.5	13.9	4.4
Digested 24.0 h	24.2	57.8	13.8	4.1
Gelose 80				
Raw	21.7	51.4	14	13.1
Digested 0.5 h	20.7	50.1	14.7	15.3
Digested 1.5 h	20.1	50.2	14.7	14.8
Digested 4.0 h	20.8	50.6	14.5	14.4
Digested 8.0 h	20.3	50.1	14.9	14.8
Digested 24.0 h	20.2	49.7	15.1	15.4

3.7. Amylopectin chain length distribution

The chain length distributions of isoamylase-debranched amylopectin from raw RMS and HAMS and their amylase digested residues are presented in Fig. 4. The debranched chains were categorised into 4 groups of different degree of polymerisation: 6–12, 13–24, 25–36 and >36 DP. Table 4 shows that among raw starches, RMS starch contained the highest proportion (32.7%) of shorter amylopectin branches (DP 6–12), with equal proportions in Gelose 50 and Gelose 80 (~21.5%). The most abundant branch length was DP 12 in RMS and DP 14 in Gelose 50 and Gelose 80. All three starches had similar proportions of DP 13–24 amylopectin branches. The proportion of amylopectin branch lengths above DP 25, e.g. DP 25–36 and DP > 36, was lower in RMS than in HAMS. The current data are similar to reported amylopectin branch length distributions in maize starches with amylose contents similar to the ones used in the current study, e.g. Du1R, *dull1* mutant (25.4%

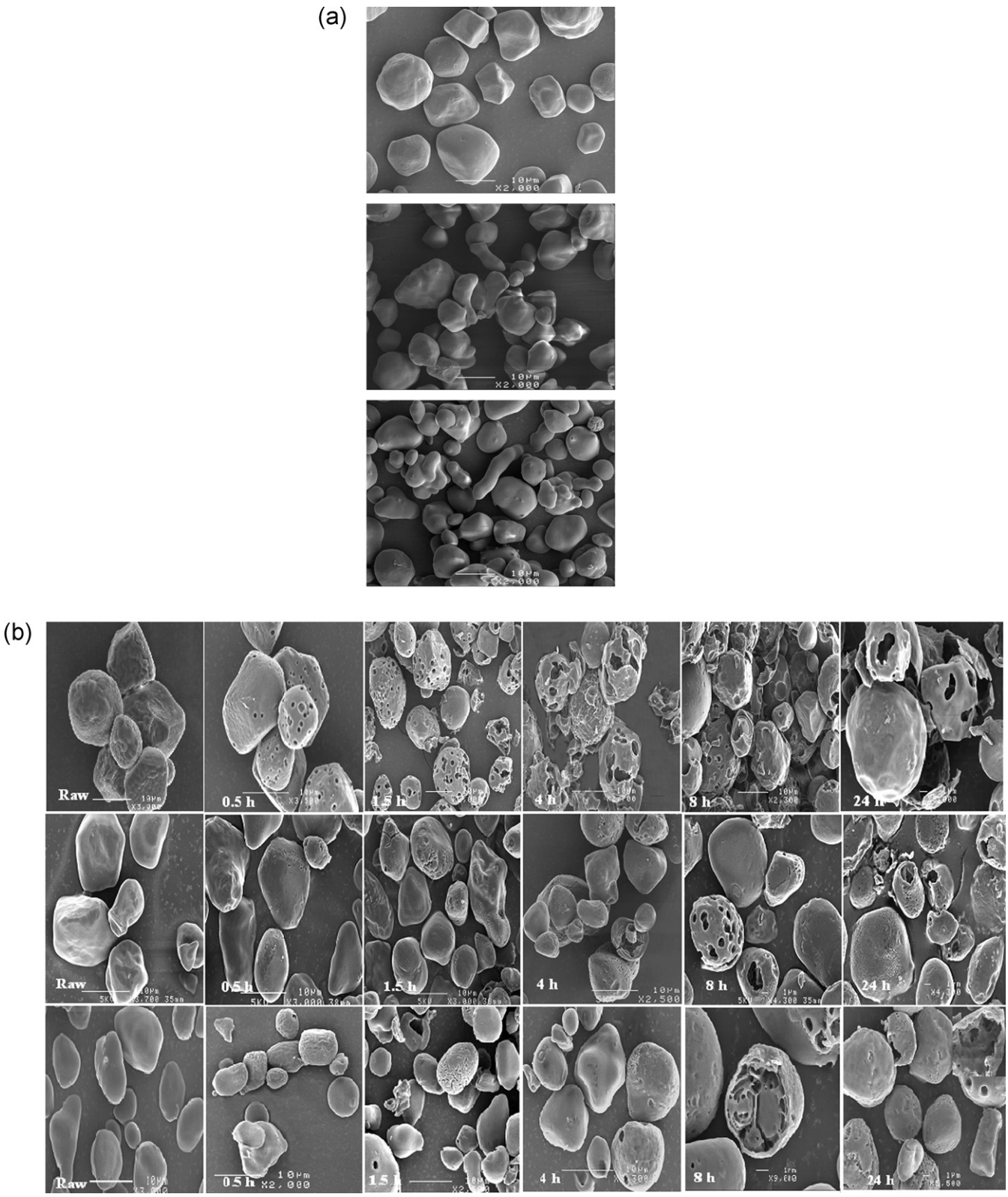

Fig. 3. (a) SEM images show numerous pores on the surface of granular regular maize starch (top image) but not G50 (middle) or G80 (lower). (b) Scanning electron micrograph (SEM) images of granular regular maize starch, Gelose 50 and Gelose 80 and their residues after different digestion times 0.0, 0.5, 1.5, 4, 8.0 and 24 h. Upper row, Regular maize starch; middle row, Gelose 50: lower row, Gelose 80.

amylose – similar to RMS) and amylose extender mutant (75.3% amylose – similar to Gelose 80) (Yao, Guiltinan, & Thompson, 2005).

In the digested RMS samples, initial enzyme hydrolysis (0.5 h) was found to decrease the proportion of long amylopectin branches (>36 DP) with a compensatory increase in other branch lengths. Changes in branch length proportions between 0.5 h and 24 h of digestion were minor despite the fact that after 24 h digestion only 3% of the starting starch was recovered (Table 1). This shows that

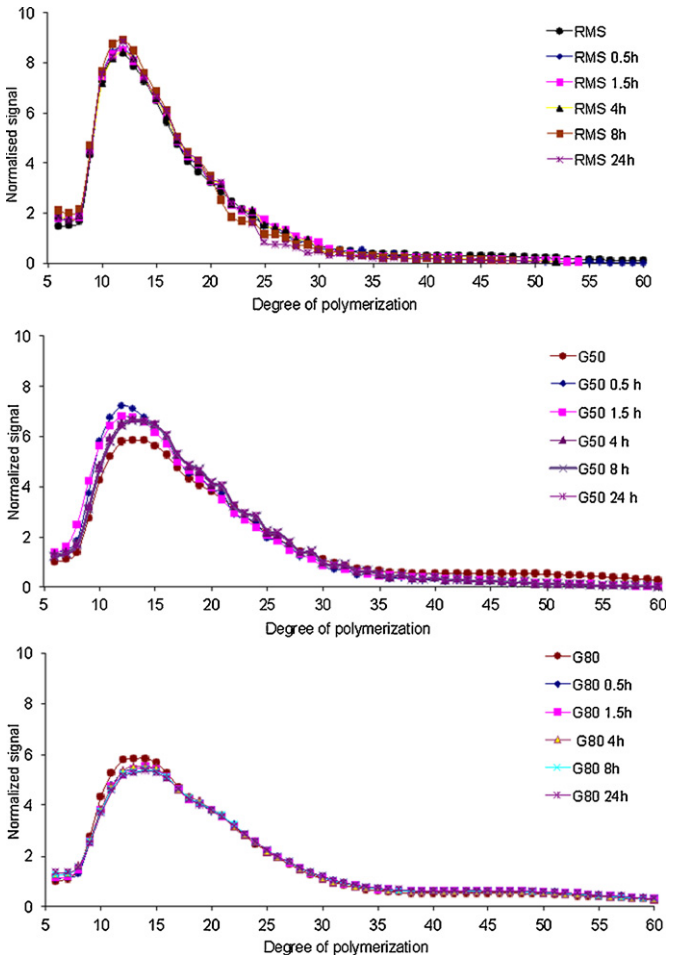

Fig. 4. Chain length distributions in debranched amylopectin of enzyme digestion residues from regular maize starch, Gelose 50 and Gelose 80.

there is no branch length specificity during the enzyme reaction as previously suggested from lower resolution analyses by Zhang et al. (2006) except for the early stages. It is possible that the sharp decrease in lamellar peak intensity (Table 2) during the initial period is connected to a preferential hydrolysis of long inter-cluster branches (DP > 36).

Initial digestion of Gelose 50 also showed a marked decrease in the proportion of long (DP > 36) branches (Fig. 4 and Table 4). Between 0.5 h and 24 h, changes in branch length proportions were much smaller but systematic (Table 4) with a decrease in short branches (<DP 13) and an increase in intermediate branch lengths (DP 13–24).

In contrast to the other two starches, Gelose 80 showed very little change in branch length proportions throughout the digestion process (Table 4). It is apparent that Gelose 50 and 80 share very similar amylopectin branch length profiles (Fig. 4). However, Gelose 80 has substantially more apparent amylose: we propose that at least some of this additional amylose is located in the inter-cluster regions, providing a barrier to enzyme access and hence preventing preferential digestion of inter-cluster amylopectin branches.

As with measurements of molecular and mesoscopic order from NMR, XRD, SAXS and DSC, amylopectin branch length profiles show only minor changes during the digestion process, consistent with a relatively non-specific attack of digestive enzymes on amylopectin structures. The exception is the preferential hydrolysis of long branches for RMS and Gelose 50 which is suggested to be due to easier access of amylase to inter-cluster regions provided there is no interference from abundant amylose as in Gelose 80.

3.8. Why are high amylose maize starch granules digested so slowly?

Despite the fact that RMS and the two HAMS are all digested by a mechanism in which there is no major preference for amylopectin branch lengths, helix form, crystallinity or lamellar organisation, the two HAMS have a markedly slower digestion rate than RMS (Fig. 1). Understanding the mechanism underlying this difference is of major significance in human nutrition and health, as granular RMS and HAMS have physiologically resistant starch contents of less than 5% and more than 50%, respectively (Bird et al., 2009). Based on the present work, it is concluded that granule architecture features with at least 100 nm scale are the primary determinant of the large differences in enzyme susceptibility of RMS and HAMS, with shorter length scales playing a secondary role as inferred from the largely invariant nature of numerous 1–10 nm scale structural measures during the digestion process (XRD, NMR, SAXS, DSC, FACE). It is most likely that it is the surface pores characteristic of RMS which are readily expanded by enzyme digestion to provide a facile entry of enzymes to the less-organised granule core for rapid digestion. In contrast, HAMS granules do not have extensive surface pores and so enzyme digestion has to proceed from the outside in with the more molecularly organised outer regions of the granule providing an effective barrier to access of enzymes to the less organised granule interior. This is consistent with previous suggestions based on more limited data sets (Evans & Thompson, 2004; Planchot et al., 1995). The fact that potato starch shows a similar microscopic enzyme digestion pattern and low granular susceptibility to amylase (Dhital et al., 2010), provides evidence that the amylose content *per se* is not responsible for the slow enzyme digestion of granular HAMS. This is consistent with evidence reported here that amylose double helix formation, as identified by a melting endotherm at >140 °C, does not occur systematically for HAMS during digestion until after 4 h by which time RMS is nearly completely digested.

HAMS and potato starch both show B-type crystallinity, and it is tempting to speculate that this is the origin for the slow digestion property of these starch granules, particularly as recrystallisation (retrogradation) of cooked starches leads to an increase in both B-type crystallinity and enzyme resistance. However, if B-type crystallinity was the direct cause of enzyme resistance, it is difficult to explain the side-by-side digestion of amorphous and crystalline material in HAMS. Furthermore, it is not always the case that A-type model crystallites are digested more rapidly than B-type crystallites. In studies of crystals from debranched amylopectins differing in polymorph through choice of crystallisation conditions, A-type crystals (Cai & Shi, 2010) showed greater enzyme resistance than B-type crystals (Cai, Shi, Rong, & Hsiao, 2010).

It is, however, possible that the presence of B-type crystallites within granules is connected with the absence of the extensive pores and channels that seem to be the origin of the quantitative difference in digestion rates between potato/high amylose and regular maize starches (Dhital et al., 2010). Based on the analogy of amylopectin as a side-chain liquid crystalline polymer (Waigh et al., 1998), B-type starches are characterised by long helical segments (due to longer branch lengths) and relatively short spacers between helices (to account for the essentially invariant 9–10 nm repeat observed by SAXS). This difference would be expected to provide more flexibility to adopt different organisational arrangements for structures containing A-type rather than B-type crystallites. Although this analogy does not explain why there are channels in RMS and other A-type cereal starches, the relative lack of

flexibility during biosynthesis does provide a rationale for the absence of channels in B-type starches.

References

Biliaderis, C. G., Page, C. M., Slade, L., & Sirett, R. R. (1985). Thermal behaviour of amylose–lipid complexes. *Carbohydrate Polymers*, *5*, 367–389.

Bird, A. R., Lopez-Rubio, A., Shrestha, A. K., & Gidley, M. J. (2009). Resistant starch *in vitro* and *in vivo*: Factors determining yield, structure, and physiological relevance. In S. Kasapis, I. T. Norton, & J. B. Ubbink (Eds.), *Modern biopolymer sciences* (pp. 449–512). London: Academic Press.

Blazek, J., & Gilbert, E. P. (2010). Investigation of structural changes during digestion of commercial starches using *in situ* small-angle neutron scatterin. *Biomacromolecules*, *11*, 3275–3289.

Blazek, J., & Gilbert, E. P. (2011). Application of small-angle X-ray and neutron scattering techniques to the characterization of starch structure: A review. *Carbohydrate Polymers*, *85*, 281–293.

Cai, L., & Shi, Y-C. (2010). Structure and digestibility of crystalline short-chain amylose from debranched waxy wheat, waxy maize, and waxy potato starch. *Carbohydrate Polymers*, *79*, 1117–1123.

Cai, L., Shi, Y-C., Rong, L., & Hsiao, B. S. (2010). Debranching and crystallization of waxy maize starch in relation to enzyme digestibility. *Carbohydrate Polymers*, *81*, 385–393.

Cairns, P., Sun, L., Morris, V. J., & Ring, S. G. (1995). Physicochemical studies using amylose as an *in vitro* model for resistant starch. *Journal of Cereal Science*, *21*, 37–47.

Castro, J. V., Ward, R. M., Gilbert, R. G., & Fitzgerald, M. A. (2005). Measurement of the molecular weight distribution of debranched starch. *Biomacromolecules*, *6*, 2260–2270.

Cooke, D., & Gidley, M. J. (1992). Loss of crystalline and molecular order during starch gelatinization – Origin of the enthalpic transition. *Carbohydrate Research*, *227*, 103–112.

Dhital, S., Shrestha, A. K., & Gidley, M. J. (2010). Relationship between granule size and *in vitro* digestibility of maize and potato starches. *Carbohydrate Polymers*, *82*, 480–488.

Eerlingen, R. C., Deceuninck, M., & Delcour, J. A. (1993). Enzyme resistant starch. II. Influence of amylose chain length on resistant starch formation. *Cereal Chemistry*, *70*, 345–350.

Evans, A., & Thompson, D. B. (2004). Resistance to alpha-amylase digestion in four native high-amylose maize starches. *Cereal Chemistry*, *81*, 31–37.

Frost, K., Kaminski, D., Kirwan, G., Lascaris, E., & Shanks, R. (2009). Crystallinity and structure of starch using wide-angle X-ray scattering. *Carbohydrate Polymers*, *78*, 543–548.

Gallant, D. J., Bouchet, B., Buleon, A., & Perez, S. (1992). Physical characteristics of starch granules and susceptibility to enzymatic degradation. *European Journal of Clinical Nutrition*, *46*, S3–S16.

Gidley, M. J., & Bulpin, P. V. (1989). Aggregation of amylose in aqueous systems-effect of chain-length on phase-behavior and aggregation kinetics. *Macromolecules*, *22*, 341–346.

Gidley, M. J., Cooke, D., Darke, A. H., Hoffmann Russell, A. L., Greenwell, P., Cooke, D., et al. (1995). Molecular order and structure in enzyme-resistant retrograded starch. *Carbohydrate Polymers*, *28*, 23–31.

Goni, I., Garcia-Diz, L., Manas, E., & Saura-Calixto, F. (1996). Analysis of resistant starch: A method for foods and food products. *Food Chemistry*, *56*, 445–449.

Hizukuri, S. (1985). Relationship between the distribution of the chain-length of amylopectin and the crystalline-structure of starch granules. *Carbohydrate Research*, *141*(2), 295–306.

Htoon, A., Shrestha, A. K., Flanagan, B. M., Lopez-Rubio, A., Bird, A. R., Gilbert, E. P., et al. (2009). Effects of processing high amylose maize starches under controlled conditions on structural organization and amylase digestibility. *Carbohydrate Polymers*, *75*(2), 236–245.

Jane, J. L., Chen, Y. Y., Lee, L. F., McPherson, A. E., Wong, K. S., Radosavljevic, M., et al. (1999). Effects of amylopectin branch chain length and amylose content on the gelatinization and pasting properties of starch. *Cereal Chemistry*, *76*, 629–637.

Jane, J. L. (2004). Starch: Structures and properties. In P. Tomasik (Ed.), *Chemical and functional properties of food saccharides* (pp. 81–101). Boca Raton, FL: CRC Press.

Jane, J. L., Kasemsuwan, T., Leas, S., Zobel, H., & Robyt, J. F. (1994). Anthology of starch granule morphology by scanning electron microscopy. *Starch/Starke*, *46*, 121–129.

Jenkins, P. J., & Donald, A. M. (1996). Application of small angle neutron scattering to the study of the structure of starch granules. *Polymer*, *37*, 5559–5568.

Jiang, G. S., & Liu, Q. (2002). Characterization of residues from partially hydrolyzed potato and high amylose corn starches by pancreatic alpha-amylase. *Starch/Starke*, *54*, 527–533.

Jiang, H., Campbell, M., Blanco, M., & Jane, J-L. (2010). Characterization of maize amylose-extender (ae) mutant starches. Part II: Structures and properties of starch residues remaining after enzymatic hydrolysis at boiling-water temperature. *Carbohydrate Polymers*, *80*, 1–12.

Jovanovich, G., & Anon, M. C. (1999). Amylose–lipid complex dissociation: A study of the kinetic parameters. *Biopolymers*, *49*, 81–89.

Li, L., Jiang, H., Campbell, M., Blanco, M., & Jane, J-L. (2008). Characterization of maize amylose-extender (ae) mutant starches. Part I: Relationship between resistant starch contents and molecular structures. *Carbohydrate Polymers*, *74*, 396–404.

Liu, H., Yu, L., Xie, F., & Chen, L. (2006). Gelatinization of corn starch with different amylose/amylopectin content. *Carbohydrate Polymers*, *65*, 357–363.

Lopez-Rubio, A., Flanagan, B. M., Gilbert, E. P., & Gidley, M. J. (2008). A novel approach for calculating starch crystallinity and its correlation with double helix content: A combined XRD and NMR study. *Biopolymers*, *89*, 761–768.

Lopez-Rubio, A., Flanagan, B. M., Shrestha, A. K., Gidley, M. J., & Gilbert, E. P. (2008). Molecular rearrangement of starch during *in vitro* digestion: Towards a better understanding of enzyme resistant starch formation. *Biomacromolecules*, *9*, 1951–1958.

Miles, M. J., Morris, V. J., & Ring, S. G. (1985). The roles of amylose and amylopectin in the gelatinization and retrogradation of starch. *Carbohydrate Research*, *135*, 257–269.

Morell, M. K., Samuel, M. S., & O'Shea, M. G. (1998). Analysis of starch structure using fluorophore-assisted carbohydrate electrophoresis. *Electrophoresis*, *19*, 2603–2611.

Morita, T., Ito, Y., Brown, I. L., Ando, R., & Kiriyama, S. (2007). *In vitro* and *in vivo* digestibility of native maize starch granules varying in amylose contents. *Journal of AOAC International*, *90*, 1628–1634.

O'Shea, M. G., Samuel, M. S., Konik, C. M., & Morell, M. K. (1998). Fluorophore assisted carbohydrate electrophoresis (FACE) of oligosaccharides: Efficiency of labelling and high-resolution separation. *Carbohydrate Research*, *307*, 1–12.

Oostergetel, G. T., & van Bruggent, E. F. G. (1993). The crystalline domains in potato starch are arranged in a helical fashion. *Carbohydrate Polymers*, *21*, 7–12.

Planchot, V., Colonna, P., Gallant, D. J., & Bouchet, B. (1995). Extensive degradation of native starch granules by alpha-amylase from *Aspergillus fumigatus*. *Journal of Cereal Science*, *21*, 163–171.

Russell, P. L. (1987). Gelatinisation of starches of different amylose/amylopectin content. A study by differential scanning calorimetry. *Journal of Cereal Science*, *6*, 133–145.

Russell, P. L., Berry, C. S., & Greenwell, P. J. (1989). Characterization of resistant starch from wheat and maize. *Cereal Science*, *9*, 1–5.

Shrestha, A. K., Ng, C. S., Lopez-Rubio, A., Blazek, J., Gilbert, E. P., & Gidley, M. J. (2010). Enzyme resistance and structural organization in extruded high amylose maize starch. *Carbohydrate Polymers*, *80*, 699–710.

Sievert, D., & Pomeranz, Y. (1989). Enzyme-resistant starch. I. Characterization and evaluation of enzymatic, thermoanalytical and microscopic methods. *Cereal Chemistry*, *66*, 342–347.

Sievert, D., & Pomeranz, Y. (1990). Enzyme-resistant starch. 2. Differential scanning calorimetry studies on heat-treated starches and enzyme-resistant starch residues. *Cereal Chemistry*, *67*, 217–221.

Srichuwong, S., Isono, N., Mishima, T., & Hisamatsu, M. (2005). Structure of lintnerized starch is related to X-ray diffraction pattern and susceptibility to acid and enzyme hydrolysis of starch granules. *International Journal of Biological Macromolecules*, *37*, 115–121.

Tan, I., Flanagan, B., Halley, P. J., Whittaker, A. K., & Gidley, M. J. (2007). A method for estimating the nature and relative proportions of amorphous, single and double-helical components in starch granules by C-13 CP/MAS NMR. *Biomacromolecules*, *8*(3), 885–891.

Themeier, H., Hollman, J., Neese, U., & Lindhauer, M. G. (2005). Structural and morphological factors influencing the quantification of resistant starch II in starches of different botanical origin. *Carbohydrate Polymers*, *61*, 72–79.

Waigh, T. A., Perry, P., Riekel, C., Gidley, M. J., & Donald, A. M. (1998). Chiral side-chain liquid-crystalline polymeric properties of starch. *Macromolecules*, *31*(22), 7980–7984.

Yao, Y., Guiltinan, M. J., & Thompson, D. H. (2005). High-performance size-exclusion chromatography (HPSEC) and flurophore-assisted carbohydrate electrophoresis (FACE) to describe the chain-length distribution of debranched starch. *Carbohydrate Research*, *340*, 701–710.

Zhang, G., Ao, Z., & Hamaker, B. R. (2006). Slow digestion property of native cereal starches. *Biomacromolecules*, *7*, 3252–3258.

Zhang, G., Zihua, A. O., & Hamaker, B. R. (2008). Nutritional property of endosperm starches from maize mutants: A parabolic relationship between slowly digestible starch and amylopectin fine structure. *Journal of Agricultural & Food Chemistry*, *56*, 4686–4694.